JACS
JOURNAL OF THE AMERICAN CHEMICAL SOCIETY
Article
pubs.acs.org/JACS

Detection of the Sn(III) Intermediate and the Mechanism of the Sn(IV)/Sn(II) Electroreduction Reaction in Bromide Media by Cyclic Voltammetry and Scanning Electrochemical Microscopy

Jinho Chang and Allen J. Bard*

Center for Electrochemistry, Department of Chemistry, University of Texas, Austin, Texas 78712, United States

Supporting Information

ABSTRACT: Fast-scan cyclic voltammetry (CV) and scanning electrochemical microscopy (SECM) were used to investigate the reduction of Sn(IV) as the hexabromo complex ion in a 2 M HBr−4 M NaBr medium. CV at scan rates to 100 V/s and SECM indicated the reaction pathway involves ligand-coupled electron transfer via an ECEC-DISP process: (1) one-electron reduction of $Sn^{IV}Br_6^{2-}$ to $Sn^{III}Br_6^{3-}$; (2) bromide dissociation of the reduced $Sn^{III}Br_6^{3-}$ to $Sn^{III}Br_5^{2-}$; (3) disproportionation of the reduced $2Sn^{III}Br_5^{2-}$ to $Sn^{IV}Br_5^{-}$ and $Sn^{II}Br_5^{3-}$; (4) one-electron reduction of $Sn^{III}Br_5^{2-}$ to $Sn^{II}Br_5^{3-}$; (5) bromide dissociation from $Sn^{II}Br_5$ to $Sn^{II}Br_4^{2-}$. The intermediate Sn(III) species was confirmed by SECM, where the Sn(III) generated at the Au tip was collected on a Au substrate in the tip generation/substrate collection mode when the distance between the tip and substrate was a few hundred nanometers.

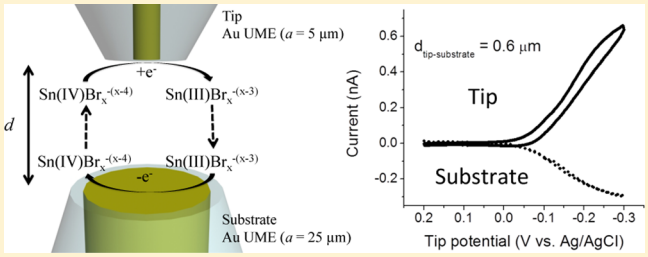

INTRODUCTION

Electrochemical reactions that involve multiple electron transfers (et's) within a single wave have long been of interest. For a reduction, when a single et step occurs, the addition of the next electron should be more difficult, e.g., for electrostatic reasons, so the next electron addition should occur at a significantly more negative potential. Thus, when a second et occurs at the same potential or even at a less negative potential than the first, this is thought to signal a significant rearrangement or a coupled chemical reaction of the product of the first et. There have thus been many studies of such apparently "simultaneous" two-et reactions, especially in metal complexes, i.e., Tl(III)/Tl(I),[1] Pt(IV)/Pt(II), Pb(IV)/Pb(II),[2] and Sn(IV)/Sn(II). Gileadi[3,4] discussed the possibility of simultaneous two-et reactions when the formation energy of an intermediate becomes larger than the energy barrier for stepwise two-et reactions. However, this model does not take into account frequent cases in which chemical reactions are coupled to the et reactions.[5] For et reactions of organic species, Evans[4] proposed the existence of intermediates during the two-et reaction, which must be able to diffuse away from the electrode surface before undergoing a second et process. For related reactions that involve at least one solid-phase species, Downard et al.[6] observed a Pd(I) intermediate during the Pd(II)/Pd(0) redox reaction and Liu et al.[2] showed a Pb(III) intermediate in the Pb(II)/PbO_2 oxidation reaction.

The electrochemical oxidation of Sn(II) was studied at Au and Pt ultramicroelectrodes (UMEs).[7] Vincente and Bruckenstein studied this reaction with a rotating Au disk electrode,[8] and Bishop and Hitchcock[9] studied electrochemical Sn(IV)−Sn(II)−Sn(0) reductions on Pt and Au electrodes. Their conclusions were that the reaction occurred by two-et reactions with no experimental evidence for the existence of an intermediate Sn(III) species. Vetter[10] and Lerner and Austin[11] proposed from kinetic measurements (by extrapolation of mass-transfer-corrected Tafel plots to zero overpotential) that the Sn(IV)/Sn(II) redox reaction occurred as two consecutive one-et steps via a Sn(III) intermediate. However, there was no direct evidence of the existence of a Sn(III) intermediate. Sn(III) has been generated by irradiation; Shinohara et al.[12] detected photogenerated Sn(III) by flash photolysis of $SnCl_2$ in hydrochloric acid, and Jiang-Tsu et al.[13] reported $Sn^{III}Cl_6^{3-}$ and $Sn^{III}Br_6^{3-}$ produced in γ-irradiated $(TMA)_2SnCl_6$ and $(TMA)_2SnBr_6$ single crystals (where TMA is $(CH_3)_4N^+$).

Fast-scan cyclic voltammetry (CV) has been used to resolve single et steps in overall two-et[6,14] and multi-et processes.[15] CV can also be used to detect unstable intermediates in electrochemical reactions.[16] A difficulty with fast-scan CV, however, is the complexity of dealing with double layer capacitance charging and adsorbed species at high scan rates (v). Since the current caused by these surface processes increases with v, while that of diffusion-controlled electrochemical reactions of dissolved species increases as $v^{1/2}$, the former dominate at large v.[15] Scanning electrochemical microscopy (SECM) has also been used as a powerful tool to detect intermediates.[17−19] A major advantage of SECM compared to fast-scan CV in this application is that the current at the tip and substrate is measured under steady-state

Received: September 30, 2013
Published: December 13, 2013

   dx.doi.org/10.1021/ja409958a | J. Am. Chem. Soc. 2014, 136, 311−320

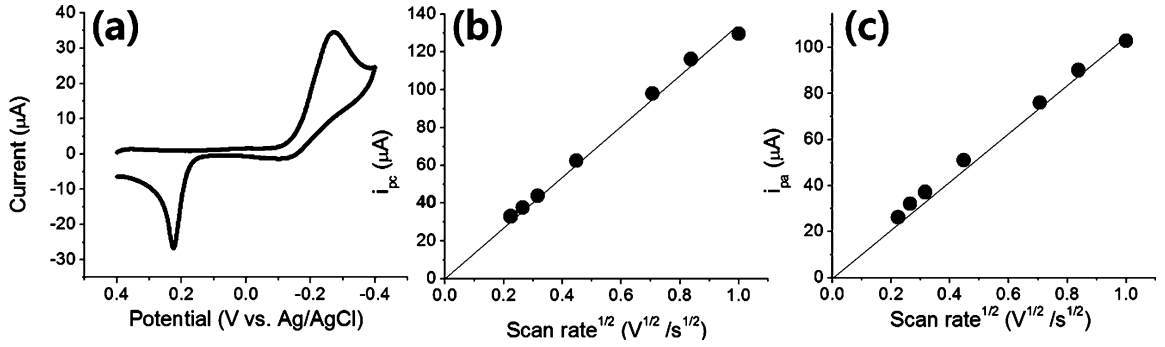

Figure 1. (a) Cyclic voltammogram in 5 mM stannic bromide in 2 M HBr + 4 M NaBr on a Au planar electrode (a = 1 mm) at 0.05 V/s and its (b) cathodic and (c) anodic peak currents versus $\nu^{1/2}$.

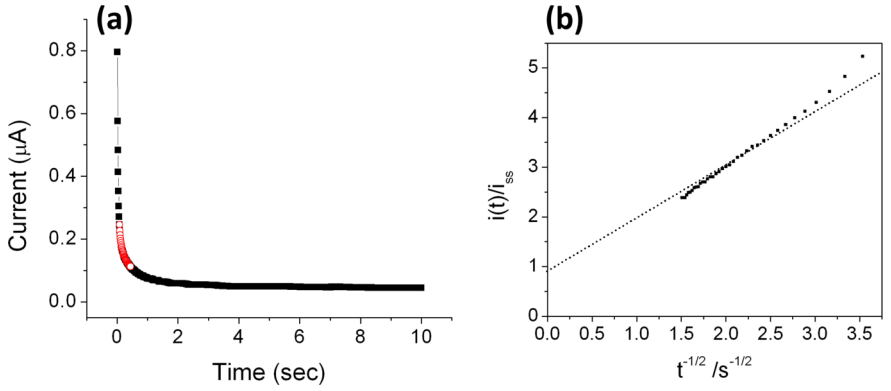

Figure 2. (a) Chronoamperogram of a Au UME (a = 50 μm) in 5 mM stannic bromide + 2 M HBr + 4 M NaBr. The potential was stepped from 0 to −0.25 V. (b) Current, $i(t)$, marked with hollow red circles in (a) divided by the steady-state current, i_{ss}, versus $1/t^{1/2}$, where t is time.

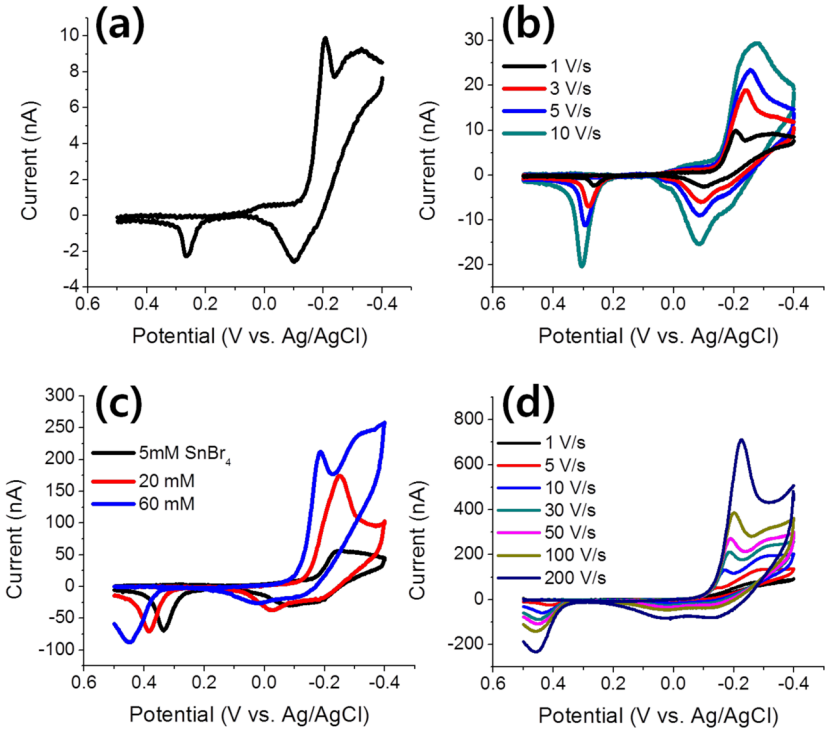

Figure 3. (a) Cyclic voltammogram in 5 mM stannic bromide at 1 V/s on a Au UME (a = 5 μm), (b) cyclic voltammograms at different ν values (1−10 V/s), (c) cyclic voltammograms with different concentrations of stannic bromide (5, 20, and 60 mM) at 50 V/s, and (d) cyclic voltammograms with 60 mM stannic bromide at different ν values (1−200 V/s). Note: the uncompensated solution resistance, R_u, was 2.5 ± 0.6 kΩ on a Au UME (a = 5 μm), and the maximum ohmic drop in 60 mM Sn(IV) solution at 200 V/s was only ∼2 mV.

dx.doi.org/10.1021/ja409958a | J. Am. Chem. Soc. 2014, 136, 311−320

conditions so that it is immune to the contribution of surface reactions of adsorbed species.[20]

We report here a study of the mechanism of the reduction of Sn(IV) in a bromide medium and the electrochemical detection of the Sn(III) intermediate in the process by fast-scan CV and SECM. This work was motivated by the desire to develop a new tin−bromine redox flow battery (RFB) which is based on Sn(IV)/Sn(II) as the anolyte and Br^-/Br_2 as the catholyte. In such an RFB both redox couples are dissolved in the same solution, so that, as in the vanadium RFB, cross-contamination is not a problem.[21] An advantage of the use of a redox species that transfers two electrons is that the capacity per unit concentration is doubled. However, the electrochemical reversibility of such redox couples that involve ligand-coupled et can be an important factor, hence the interest in probing the reaction mechanism and attempting to improve reversibility.

EXPERIMENTAL SECTION

Chemicals. All solutions were prepared with deionized Milli-Q water, and the chemicals were stannic bromide ($SnBr_4$; 99%), sodium bromide (NaBr; ≥99.0%), and ferrocenemethanol (FcMeOH; 97%) from Sigma-Aldrich and hydrobromic acid (HBr; 47−49%) and sodium nitrate ($NaNO_3$; ≥99%) from Fisher Scientific.

Instruments and Measurements. Fast-scan-rate CV and chronoamperometry were performed with a CH 660 workstation (CH Instruments, Austin, TX), and SECM was carried out with a CH 900 SECM bipotentiostat (CH Instruments). All CV measurements were performed with three electrodes at room temperature: gold disks with different radii, a (1 mm, 50, 25, and 5 μm), as working electrodes, a carbon rod as a counter electrode, and Ag/AgCl (in saturated KCl) as a reference electrode. Gold disk electrodes were cleaned in 0.1 M H_2SO_4 solution by 50 successive cycles from −0.25 to +1.5 V at v = 0.05 V/s before electrochemical measurements were performed. All solutions were purged with argon for 20 min before each experiment, and Ar was kept flowing over the solutions during electrochemical measurements to minimize diffusion of oxygen into the solutions. Simulations of linear sweep voltammograms were performed by DigiElch, the commercial simulation software (DigiElch-Professional v6.F, ElchSoft.com).

Gold UMEs. A gold (99.99%) wire from Goodfellow (Devon, PA) and a borosilicate capillary with an outer diameter of 1.5 mm and inner diameter of 0.75 mm from FHC (Bowdoin, ME) were used to fabricate UMEs by procedures described elsewhere.[22] For chronoamperometry and fast-scan CV experiments, Au UMEs were used without polishing down the insulating glass to obtain a small RG (ratio of the radius of the insulating material to that of the metal disk). In SECM experiments, Au UMEs with a = 5 or 25 μm were sharpened to obtain an RG of 1.1−2 to allow the tip to approach a substrate electrode as closely as possible without touching it. In the SECM experiment for detecting and collecting Sn(III), the Au UME (a = 5 μm) as the tip was electrodeposited with Au to fill a metal recession to approach a tip to substrate distance, d, of 600 nm as described in a previous paper.[23]

RESULTS AND DISCUSSION

Cyclic Voltammetry. Figure 1a shows a CV scan with a gold planar electrode (a = 1 mm) at 0.05 V/s in 5 mM stannic bromide + 2 M HBr + 4 M NaBr. The separation of the cathodic and anodic peaks, ΔE_p, was about ~0.5 V, indicating large irreversibility. Both the cathodic and anodic peaks were proportional to the square root of the scan rate, $v^{1/2}$ (Figure 1b,c) for $v \leq 1$ V/s, meaning both involved diffusion-controlled reactions.

The diffusion coefficient, D, of the dissolved Sn(IV)−Br^- species ($SnBr_6^{2-}$) was measured by chronoamperometry at a Au UME (a = 50 μm), where D can be obtained without knowledge of the concentration of electroactive species.[24]

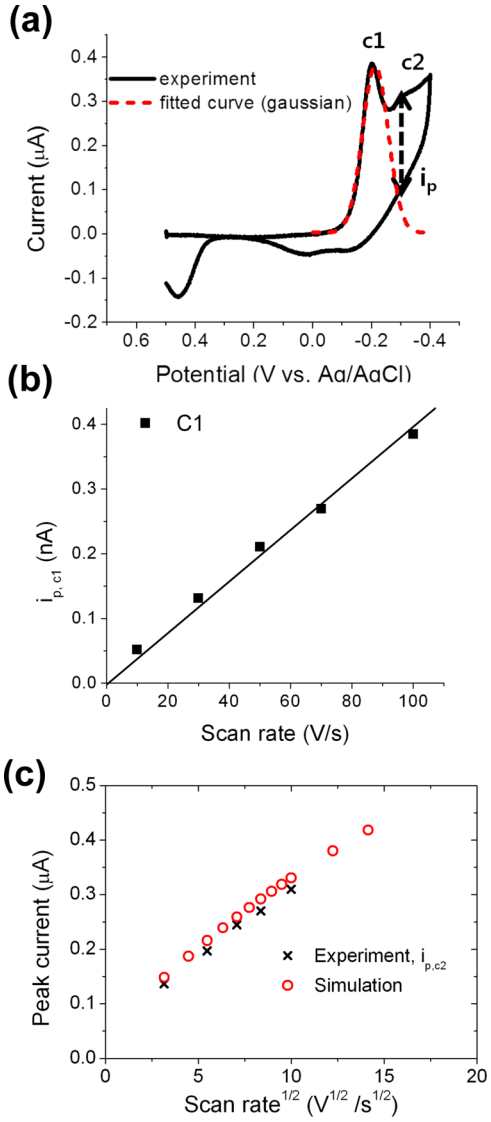

Figure 4. (a) Cyclic voltammogram in 60 mM stannic bromide + 2 M HBr + 4 M NaBr at 100 V/s (black line) and Gaussian curve for fitting the surface peak, c1 (red line), (b) peak currents of c1 vs v, and (c) peak currents of c2 (black times signs) and reduction peak currents from the simulation (red circles) vs $v^{1/2}$. The simulated linear sweep voltammograms are shown in Figure S3, Supporting Information, and the reactions and corresponding parameters are listed in Table S1, Supporting Information.

Figure 2a shows a chronoamperogram where the potential was stepped from 0 to −0.25 V, the reduction potential where the current reached a steady state. The current at a disk UME is composed of two parts, a transient and a steady-state region:

$$i_d(t) = \pi^{1/2} nFD^{1/2} C^* a^2 t^{-1/2} + 4nFDC^* a \quad (1)$$

$$i_d(t)/i_{d,ss} = (\pi^{1/2}/4)a(Dt)^{-1/2} + 1 \quad (2)$$

where n is the overall electron number, F is the Faraday constant, a is the radius of the UME, C^* is the bulk concentration of reactant, and $i_{d,ss}$ is the steady-state current. To obtain the diffusion coefficient, one can obtain the most precise value for times that are sufficiently long that there is no contribution from double layer charging, but still also not near the steady-state region. Therefore, a region shown by red circles

dx.doi.org/10.1021/ja409958a | J. Am. Chem. Soc. 2014, 136, 311−320

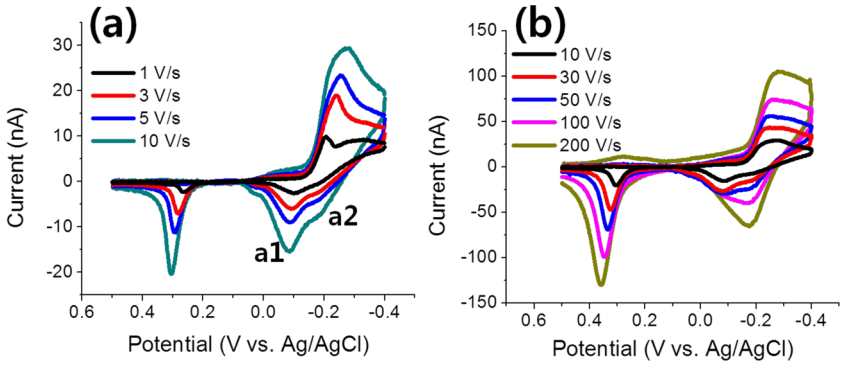

Figure 5. Cyclic voltammograms on a Au UME (a = 5 μm) in 5 mM stannic bromide + 2 M HBr + 4 M NaBr at different v values: (a) 1−10 V/s and (b) 10−200 V/s.

Table 1. Peak Potentials of UPD of Sn(0) and Its Oxidation in Different Conditions[a]

		E_p (vs NHE)			
no.	electrolyte	oxidation	reduction	obsd v (V/s)	ref
1	0.1 mM $Sn^{II}Cl_2$ + 4 M HCl	0.09	0.09	0.1	8
2	10 mM $Sn^{II}SO_4$ + 1 M H_2SO_4	0.16	0.14	0.01	27
3	0.1 M $Sn^{II}Cl_2$ + 1 M HCl	0.15	0.09	0.02	28
4	0.3 mM $Sn^{II}SO_4$ + 0.5 M H_2SO_4	0.15	0.17	0.05	29
	5 mM $Sn^{IV}Br_4$ + 2 M HBr + 4 M NaBr	0.09	0.07	1	this work

[a]In all experiments, a polycrystalline Au electrode was used as the working electrode, and peak potentials are reported with respect to the normal hydrogen electrode (NHE), with the potential vs the Ag/AgCl reference electrode being 0.20 V more negative.

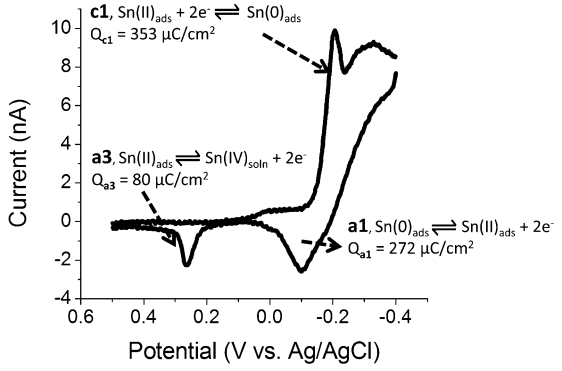

Figure 6. Cyclic voltammogram in 5 mM stannic bromide on a Au UME (a = 5 μm) at 1 V/s with assigned surface peaks and corresponding reactions.

was used for an estimation of D. From the chronoamperogram, a plot of the experimental ratio $i(t)/i_{ss}$ as a function of $t^{-1/2}$ was obtained, and its slope and intercept were 0.99 and 0.97, respectively. The following equation is a more precise expression of the current at a microdisk electrode at a given time:[24]

$$i_d(t)/i_{d,ss} = (2/\pi^{3/2})a(Dt)^{-1/2} + 1 \quad (3)$$

The calculated D of $SnBr_6^{2-}$ in 2 M HBr + 4 M NaBr was 3.2 × 10^{-6} cm^2/s, and n was calculated from the known C to be 2.1 from the following equation (i_{ss} = 67 nA in Figure 2a):

$$i_{ss} = 4nFC^*Da \quad (4)$$

This characterization confirms the cathodic and anodic CV peaks can be attributed to the Sn(IV)/Sn(II) redox reaction.

Fast-Scan Cyclic Voltammetry. A Au UME (a = 5 μm) was used as a working electrode to reduce the iR drop,[25] and cyclic voltammograms measured in the background solution (2 M HBr + 4 M NaBr) were subtracted from all cyclic voltammograms measured in the solutions with stannic bromide at fast scan rates to minimize the large charging currents at high v. An example is shown in the Supporting Information, Figure S1.

Figure 3a shows a cyclic voltammogram in 5 mM stannic bromide at 1 V/s where three sharp peaks are observed, one cathodic and two anodic, in addition to a typical peak for a dissolved species. At this UME (a = 5 μm), a purely diffusion-controlled reaction of a dissolved reactant should produce a quasi-steady-state response with almost no reversal peaks at 1 V/s as shown in the simulation result depicted in the Supporting Information, Figure S2. In this scan the three sharp peaks were generated from surface reactions of adsorbed species. The origins of the surface peaks will be discussed in the next section.

In the cathodic region of the cyclic voltammogram shown in Figure 3a, two peaks, one at −0.2 V and the other at −0.3 V, represented as c1 and c2, appeared separate at v = 1 V/s. When v was increased to 3 V/s (Figure 3b) with small Sn(IV) concentrations (5−10 mM), the two cathodic peaks started to merge, and when v reached 10 V/s, only a single wave could be discerned. As the Sn(IV) concentration was increased to 60 mM, the two peaks still remained separate even at 50 V/s (Figure 3c), finally merging, however, at 200 V/s (Figure 3d). The two cathodic peaks in 60 mM stannic bromide solution were analyzed up to 100 V/s, which was the maximum v to observe them. The peak currents of c1 were proportional to v (Figure 4b), indicating a surface reaction, which is also consistent with the symmetrical peak shape.[26] The peak currents of c2 at different v values were measured by subtraction of the c1 peaks, assuming a Gaussian shape as shown in Figure 4a. The linear sweep voltammograms for a 5 μm radius UME of the diffusion-controlled Sn(IV) reduction were simulated from the proposed reaction pathway, discussed later in the mechanism section, using the parameters reported there (Supporting Information, Figure S3). The peak currents measured from the simulated linear sweep voltammograms as a function of $v^{1/2}$ fit well with those of c2, and this evidence supports the proposed reaction mechanism of Sn(IV) reduction

dx.doi.org/10.1021/ja409958a | J. Am. Chem. Soc. 2014, 136, 311−320

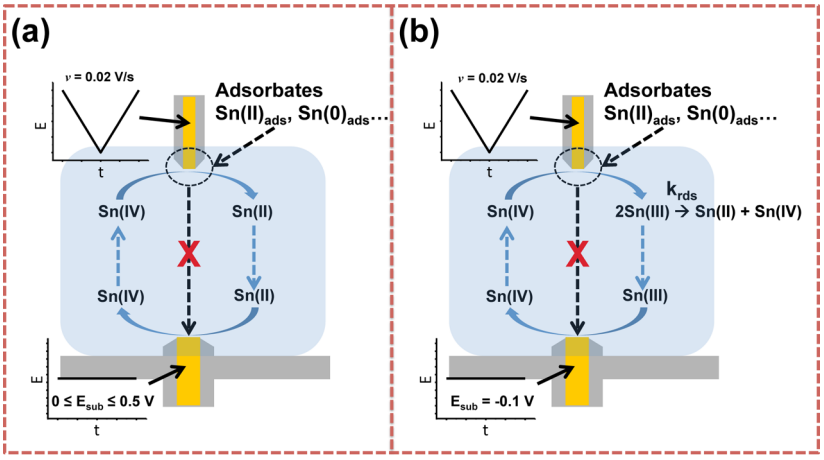

Figure 7. Depiction of the detection of (a) Sn(II) and (b) intermediate Sn(III) through the TG/SC mode in SECM. The substrate was a Au UME (a = 25 μm), and the tip was a Au UME (a = 5 μm). The substrate was held at a constant potential, while the tip potential was scanned at a scan rate of 0.02 V/s.

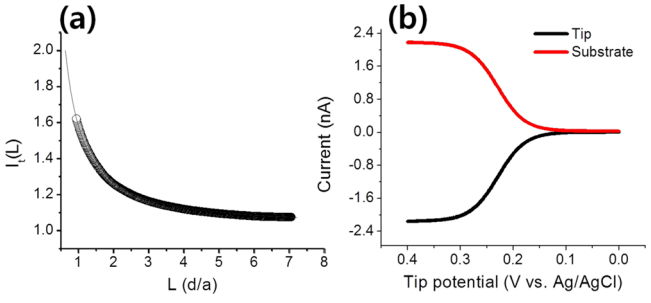

Figure 8. (a) Dimensionless current, $i_t(L)$ (steady-state tip current, i_{ss}, divided by the steady-state tip current at d = infinite, $i_{ss,\ infinite}$) versus L (d/a) in 1 mM FcMeOH + 0.1 M $NaNO_3$. The hollow circles represent the experimental plot, and the solid line represents the theoretical curve. (b) Cyclic voltammogram of the tip at 0.02 V/s (black line) and corresponding current of the substrate held at 0 V_{sub} (red line).

involving Sn(III) as an intermediate. In the SECM section, we will further discuss the collection of the Sn(III)−bromide intermediate in SECM experiments, which also supports the proposed reaction pathway.

The anodic region on scan reversal was characterized by three anodic waves as shown in Figure 4a, with a1 and a2 in the region of 0 to −0.2 V and a3 at 0.3 to 0.4 V; these were also investigated as a function of ν. Peak a1, which was observed at −0.1 V in 5 mM Sn(IV) solution at ν = 1 V/s (Figure 3a), is caused by a surface reaction. As ν increased to 3 V/s, a shoulder at −0.2 V emerged (a2) and grew as ν increased as shown in Figure 5a. However, when ν became 50 V/s, the two peaks started to merge, and the peaks were completely combined at 200 V/s (Figure 5b). The peak currents of a1 were proportional to ν over the range of 1−10 V/s. The peak currents of a2 were not proportional to ν. However, it was also difficult to show it was a diffusion-controlled reaction because the scan rate range from 1 to 10 V/s was not fast enough to attain semi-infinite diffusion at the UME with a = 5 μm, to obtain the classic CV behavior where peak currents are linearly proportional to $\nu^{1/2}$.[25] Therefore, like the case of c2, the analysis of a2 was also hindered because of the surface peak, a1.

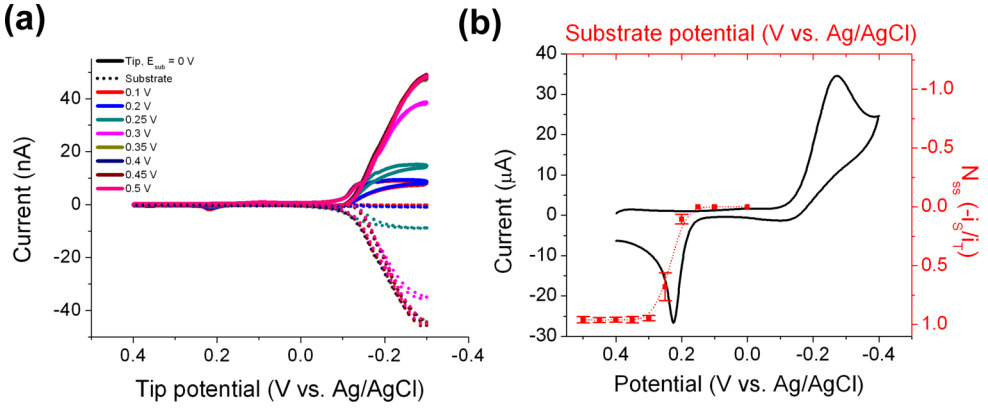

Figure 9. (a) Cyclic voltammograms of the tip in 5 mM stannic bromide + 2 M HBr + 4 M NaBr at 0.02 V/s (solid lines) and corresponding currents of the substrate held at different substrate potentials (dotted lines). In the substrate cyclic voltammograms, background currents were subtracted. Potentials constantly applied to the substrate were varied from 0 to 0.5 V_{sub}. (b) Cyclic voltammogram in 5 mM stannic bromide + 2 M HBr + 4 M NaBr on a Au planar electrode (a = 1 mm) at 0.05 V/s (black line) and N_{ss} measured in the TG/SC mode of SECM at different substrate potentials (red line). The results (squares) represent the average of three experiments to determine N_{ss}, and the standard deviation is shown as an error bar.

dx.doi.org/10.1021/ja409958a | J. Am. Chem. Soc. 2014, 136, 311−320

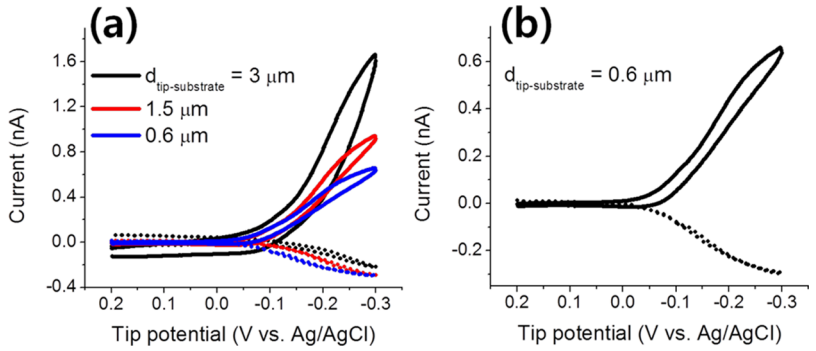

Figure 10. (a) Tip voltammograms (solid lines) and corresponding background-subtracted substrate currents (dotted lines) in 5 mM stannic bromide + 2 M HBr + 4 M NaBr with different d values and (b) tip/substrate voltammograms at d = 600 nm. The substrate was held at −0.1 V, and the tip was scanned from +0.2 to −0.3 V_{tip} at 0.02 V/s.

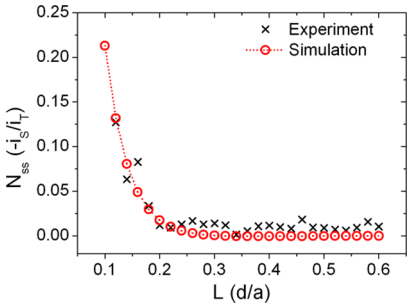

Figure 11. Collection efficiency, N_{ss} ($-i_S/i_T$), measured by an experiment (black) at E_{tip} = −0.13 V and E_{sub} = −0.1 V and simulations (red) versus L (d/a). The reactions and corresponding parameters in the simulation are listed in Table 2.

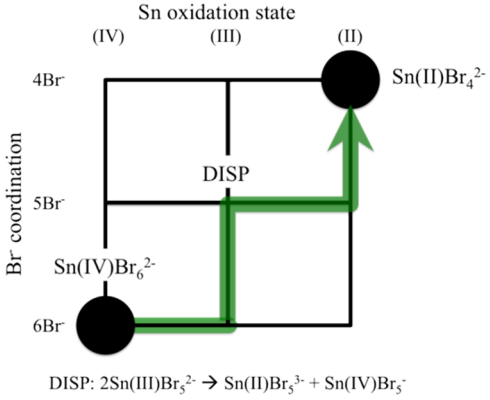

Figure 12. Schematic description of the possible reaction pathway during $Sn^{IV}Br_6^{2-}/Sn^{II}Br_4^{2-}$ reduction in 2 M HBr + 4 M NaBr.

Origin of the Surface Peaks. The surface peaks shown in Figure 3a, one cathodic at −0.2 V (c1) and the others anodic at −0.1 V (a1) and 0.25 V (a3), have been discussed previously. Vincente and Bruckenstein[8] proposed that underpotential deposition (UPD) of Sn(0) on gold from a Sn(II) solution in 4 M HCl is associated with c1 with its oxidation at −0.15 V vs SCE (a1). Other references also describe the UPD of Sn(0) in different Sn(II) solutions, as listed in Table 1.[8,27−29] The potentials of surface peaks c1 and al observed under our conditions for the Sn(IV)−Br^- system are comparable to the reported potentials for UPD of Sn(0) and its oxidation. Charges estimated by integration of the peaks were 353 (Q_{c1}), 272 (Q_{a1}), and 80 (Q_{a3}) μC/cm^2, so $Q_{c1} \cong Q_{a1} + Q_{a3}$. This result agrees with the conclusion for the Sn(II)−Cl^- [8] that the underpotentially deposited Sn(0) (corresponding to c1) was oxidized to $Sn(II)_{ads}$ (a1) and $Sn(II)_{ads}$ was oxidized to the soluble Sn(IV) species (a3) (note that the soluble Sn(II) species started to be oxidized at 0.2 V as confirmed by SECM experiments, discussed in the next section. Note also that the oxidation peak in Figure 1a is sharp, but the peak currents are proportional to $v^{1/2}$ (0.05−1 V/s) because both diffusing and adsorbed Sn(II) species that are oxidized to soluble Sn(IV) contribute to this peak. About 1/2 monolayer coverage was estimated from a calculation of the equivalent charge of a monolayer of Sn by assuming a close-packing arrangement of Sn^{2+} ions (ionic radius 122 pm), a two-et, and the absence of

Table 2. Reaction Mechanisms and Corresponding Relevant Time-Dependent Diffusion Equations in Cylindrical Coordinates[a]

Reactions and parameters	
A + e⁻ ⇋ B	E^0 = -0.25 V, α = 0.5, k_{et} = 0.1 cm/s
B → C	k_1 = 6.9 x 10^3 s^{-1}
2C → D + F	k_{disp} = 1.0 x 10^5 M^{-1}s^{-1}
C + e⁻ ⇋ D	E^0 = -0.11 V, α = 0.5, k_{et} ≥ 10 cm/s
D → E	k_2 = 2.0 x 10^4 s^{-1}
F → A	k_3 = 2.0 x 10^4 s^{-1}

Relevant time-dependent diffusion equations

$$(1)\ \frac{\partial C_A}{\partial t} = D_A\left[\frac{\partial^2 C_A}{\partial r^2} + \frac{1}{r}\frac{\partial C_A}{\partial r} + \frac{\partial^2 C_A}{\partial z^2}\right] + k_3 C_F$$
$$(2)\ \frac{\partial C_B}{\partial t} = D_B\left[\frac{\partial^2 C_B}{\partial r^2} + \frac{1}{r}\frac{\partial C_B}{\partial r} + \frac{\partial^2 C_B}{\partial z^2}\right] - k_1 C_B$$
$$(3)\ \frac{\partial C_C}{\partial t} = D_C\left[\frac{\partial^2 C_C}{\partial r^2} + \frac{1}{r}\frac{\partial C_C}{\partial r} + \frac{\partial^2 C_C}{\partial z^2}\right] - k_{disp} C_C^2$$
$$(4)\ \frac{\partial C_D}{\partial t} = D_D\left[\frac{\partial^2 C_D}{\partial r^2} + \frac{1}{r}\frac{\partial C_D}{\partial r} + \frac{\partial^2 C_D}{\partial z^2}\right] + \frac{1}{2}k_{disp} C_C^2 - k_2 C_D$$
$$(5)\ \frac{\partial C_E}{\partial t} = k_2 C_D$$
$$(6)\ \frac{\partial C_F}{\partial t} = +\frac{1}{2}k_{disp} C_C^2 - k_3 C_F$$

The initial condition, completing the definition of the problem

t = 0, all r, z: $C_A = C_A^* = 5$ mM, $C_{B-E} = 0$, $D_{A-E} = 3.2 \times 10^{-6}$ cm^2/s
E_{tip} = -0.3 V, E_{sub} = 0 V

The current on the tip (i_T) and the substrate (i_S)

$$i_T = 2\pi F D_A \int_0^a \left(\frac{\partial C_A}{\partial z}\right)_{z=0} r dr + 2\pi F D_C \int_0^a \left(\frac{\partial C_C}{\partial z}\right)_{z=0} r dr$$

$$i_S = 2\pi F D_B \int_0^a \left(\frac{\partial C_B}{\partial z}\right)_{z=0} r dr + 2\pi F D_D \int_0^a \left(\frac{\partial C_D}{\partial z}\right)_{z=0} r dr$$

[a] r and z are the coordinates in the radial and normal directions to the electrode surface at its center, respectively, D_i and C_i are the diffusion coefficient and concentration of the species [i = A, B, C, D, E, and F), and t is time. Species i: (A) $Sn^{IV}Br_6^{2-}$; (B) $Sn^{III}Br_6^{3-}$; (C) $Sn^{III}Br_5^{2-}$; (D) $Sn^{II}Br_5^{3-}$; (E) $Sn^{II}Br_4^{2-}$; (F) $Sn^{IV}Br_5^-$].

dx.doi.org/10.1021/ja409958a | J. Am. Chem. Soc. 2014, 136, 311−320

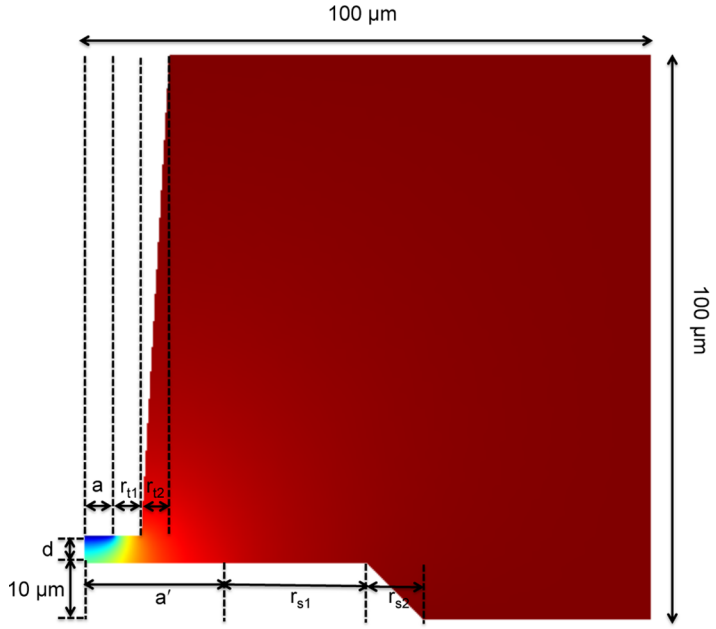

No.	z coordinate	r coordinate	Boundary conditions
1	10 μm + d	$0 \le r \le a$	$C_A = 0$, $D_A\frac{\partial C_A}{\partial z} = -D_B\frac{\partial C_B}{\partial z}$
2	10 μm + d	$a \le r \le r_{t1}$	$D_A\frac{\partial C_A}{\partial z} = D_B\frac{\partial C_B}{\partial z} = 0$
3	10 μm + $d \le z \le$ 100 μm	$r_{t1} \le r \le r_{t2}$	$D_A\frac{\partial C_A}{\partial z} = D_B\frac{\partial C_B}{\partial z} = 0$
4	100 μm	$r_{t2} \le r \le$ 100 μm	$C_A = C_A^*$; $C_B = 0$
5	10 μm	$0 \le r \le a'$	$C_B = 0$, $D_B\frac{\partial C_B}{\partial z} = -D_A\frac{\partial C_A}{\partial z}$
6	10 μm	$a' \le r \le r_{s1}$	$D_A\frac{\partial C_A}{\partial z} = D_B\frac{\partial C_B}{\partial z} = 0$
7	10 μm	$r_{s1} \le r \le r_{s2}$	$D_A\frac{\partial C_A}{\partial z} = D_B\frac{\partial C_B}{\partial z} = 0$
8	$0 \le z \le$ 10 μm	$r_{s2} \le r \le$ 100 μm	$C_A = C_A^*$; $C_B = 0$
9	$0 \le z \le$ 100 μm	$r =$ 100 μm	$C_A = C_A^*$; $C_B = 0$
10	$0 \le z \le$ 100 μm	$r = 0$	$D_A\frac{\partial C_A}{\partial r} = D_B\frac{\partial C_B}{\partial r} = 0$

Figure 13. Two-dimensional axial symmetry dimension image with parameters (left) and boundary conditions (right) in an SECM simulation.

bromide adsorption. Mao et al.[30] studied UPD of Sn on a Au(111) electrode in 1 mM $SnSO_4$ + 0.5 M H_2SO_4 and reported ~0.7 monolayer coverage, in reasonable agreement with our estimate. From the above considerations, Sn(0) could be underpotentially deposited from the Sn(IV) solution in the following reactions indicated on the cyclic voltammogram in Figure 6:

$$Sn(IV)_{soln} + 2e^- \rightleftharpoons Sn(II)_{soln}\ (c2) \quad (5)$$

$$Sn(II)_{soln} \rightleftharpoons Sn(II)_{ads} \quad (6)$$

$$Sn(II)_{ads} + 2e^- \rightleftharpoons Sn(0)_{ads}\ (c1) \quad (7)$$

$Sn(0)_{ads}$ can also be formed through another pathway, i.e., disproportionation of adsorbed Sn(II).[29] Here irreversible adsorption of Sn(II) on a gold surface by immersing a gold electrode into 1 mM $SnSO_4$ + 0.5 M H_2SO_4 solution at open circuit leads to irreversibly adsorbed $Sn(0)_{ads}$ via a disproportionation reaction of Sn(II) on the gold surface:

$$2Sn(II)_{ads}(Au) \rightleftharpoons Sn(IV)_{soln} + Sn(0)_{ads}(Au) \quad (8)$$

The potential to oxidize this Sn(0) was almost the same as that of $Sn(0)_{ads}$ formed through UPD.[31]According to mixed potential theory,[32] the oxidation from Sn(II) to Sn(IV) and the reduction from Sn(II) to Sn(0) can occur simultaneously by transferring electrons from the oxidation to the reduction reaction through the conductive Au surface. The equilibrium constant, K_{disp}, of the disproportionation of $Sn(II)_{ads}$ in reaction 8 could be obtained from the difference, ΔE°, in the formal potentials of reactions 5 and 7, $E_1^{\circ\prime}$ and $E_2^{\circ\prime}$, from the following equation:

$$\ln K_{disp} = -(nF/RT)(E_1^{\circ\prime} - E_2^{\circ\prime}) \quad (9)$$

where R is the gas constant and T is the temperature. ΔE° was roughly estimated from the difference in the half peak potential, $E_{1/2}$, of reactions 5 and 7 in Figure 3a, and K_{disp} was calculated to be 5.2×10^3. Therefore, it was also possible to form the underpotentially deposited Sn(0) via the spontaneous disproportionation of $Sn(II)_{ads}$, which was generated from the electrochemical reduction of Sn(IV) through the reaction pathway of reaction 5 → reaction 6 → reaction 8.

SECM Studies. Fast-scan CV is a useful technique for elucidating reaction mechanisms, but suffers from an extreme sensitivity to surface processes of adsorbed intermediates that can dominate the response at high scan rates. Thus, it is difficult to study the Sn(IV) to Sn(II) reaction in the presence of the adsorbed species described above. SECM does not suffer from this problem, since measurements can be made at steady state; transient currents from adsorbed species do not perturb these SECM measurements. In SECM, the distance between the tip and substrate, d, controls the time it takes for the species to diffuse across the gap and provide kinetic information. For example, the transiently existing Sn(III) can be detected at small d values, but not at larger ones.

Schemes of tip generation/substrate collection (TG/SC) mode of SECM in 5 mM Sn(IV) + 2 M HBr + 4 M NaBr are shown in Figure 7. The tip potential was scanned from a positive one in the negative direction for the reduction of Sn(IV) at the Au tip UME (a = 5 μm), while different constant potentials were applied to the Au substrate UME (a = 25 μm) to reoxidize reduced Sn(IV) species. In this case, the surface-controlled reactions of $Sn(II)_{ads}$ and $Sn(0)_{ads}$ on the tip do not perturb the steady-state solution reactions on the substrate, and therefore, the diffusive Sn(II) and Sn(III) generated by the reduction of Sn(IV) on the tip can be collected on the substrate without interference from surface reactions. To maximize the collection efficiency, N_{ss}, of Sn(II) and Sn(III) in the TG/SC mode, the N_{ss} of a purely diffusion-controlled redox mediator should be close to 100% at a small distance between the tip and substrate. To check this with the present configuration, 1 mM FcMeOH in 0.1 M $NaNO_3$ solution was chosen as a stable redox mediator. In this experiment, constant potentials of 0.4 and 0 V were applied on the tip and the substrate, respectively, to oxidize FcMeOH at the tip and reduce the oxidized FcMeOH at the substrate. This produces a positive feedback response (hollow circles in Figure 8a) as a function of the

dx.doi.org/10.1021/ja409958a | J. Am. Chem. Soc. 2014, 136, 311−320

dimensionless distance, $L = d/a$, that followed the theoretical positive feedback curve (solid line in Figure 8a).[33] The tip was held at $d = 5$ μm ($L = 1$), and E_{tip} was scanned from 0 to 0.4 V while the substrate was held at an E_{sub} of 0 V: N_{ss} from the tip and substrate currents at $E_{tip} = 0.4$ V was essentially 1.0 (Figure 8b). Previous studies[34] showed that $N_{ss} > 0.99$ when $d/a < 2$ and $d/a \ll R_s$, where R_s is r_s/a (r_s is the radius of the substrate electrode). R_s in our SECM setup was 5.

Maintaining the $d = 5$ μm gap, we changed the solution from 1 mM FcMeOH to 5 mM Sn(IV) + 2 M HBr + 4 M NaBr, and E_{tip} was scanned from +0.4 to −0.3 V while E_{sub} was held at different constant potentials from 0 to 0.5 V (the scheme depicted in Figure 7a). Cyclic voltammograms of the tip and corresponding substrate currents (i_{tip} and i_{sub}) at different E_{sub} values shown in Figure 9a yielded TG/SC voltammograms and N_{ss}. These i_{tip} and i_{sub} values at $E_{tip} = -0.3$ V are plotted vs E_{sub} (red line with boxes in Figure 9b), with the cyclic volammogram on the Au planar electrode with $a = 1$ mm at 0.05 V/s overlaid on the N_{ss} plot. The reduced species on the tip was collected on the substrate from $E_{sub} = 0.2$ V, and N_{ss} reached 100% at $E_{sub} = 0.3$ V. The N_{ss} given at this substrate potential range followed well the oxidation of Sn(II) to Sn(IV) in the cyclic voltammogram and shows that the solution-phase Sn(II) species produced by reduction at the tip is oxidized at $E_{sub} = 0.2$ V and beyond without any irreversible decomposition reactions to electroinactive species within a time scale $\tau = 85$ ms.[34] Note this measurement is not perturbed by formation of adsorbed species, which are not detected at steady state.

To collect any intermediates in the reduction process, such as Sn(III), the applied E_{sub} must be negative of the values where Sn(II) is oxidized; thus, $E_{sub} = -0.1$ V was applied to the substrate while the tip was scanned from $E_{tip} = +0.2$ to $E_{tip} = -0.3$ V, as illustrated in Figure 7b. The results of this experiment are shown in Figure 10. To detect an intermediate at the substrate, d must be sufficiently small that the time required for diffusion of the generated intermediate, Sn(III), from tip to substrate is shorter than the lifetime of the intermediate. As discussed below, Sn(III) can be removed by disproportionation:

$$2\mathrm{Sn(III)} \rightleftharpoons \mathrm{Sn(IV)} + \mathrm{Sn(II)} \quad (10)$$

In addition, in the overall reaction from $SnBr_6^{2-}$ to $SnBr_4^{2-}$, one must account for loss of Br^- ligands. The oxidation current at the substrate is attributed to the oxidation of Sn(III) to Sn(IV). To position the tip close to the substrate without crashing it, it is useful to have the metal protrude very slightly from the glass insulation.[23,35] This was achieved by electrodeposition of Au, and the minimum $d \approx 600$ nm was achieved as measured by positive feedback in FcMeOH solution.[23]

Figure 10a shows cyclic voltammograms of the tip (solid lines) and corresponding currents of the substrate held at −0.1 V (dotted lines) as a function of d. In the substrate cyclic voltammograms, background generated from Sn(IV) reduction was subtracted. At $d = 3$ μm, Sn(IV) started to be reduced at $E_{tip} = -0.05$ V, while a small oxidation current started to flow at the substrate. The substrate current resulted from the collection of intermediates, e.g., a Sn(III) species, a probable candidate, generated from the Sn(IV) reduction. This was not seen when the same experiments were carried out with only the background solution. Figure S4 in the Supporting Information shows a TG/SC cyclic voltammogram in 2 M HBr + 4 M NaBr without Sn(IV) solution at $d = 3$ μm and $E_{sub} = -0.1$ V, where there was no current collected on the substrate. At $d = 0.6$ μm (the enlarged cyclic voltammogram is shown in Figure 10b), the potential where the oxidation started on the substrate moved to −0.05 V_{tip} and the collected current was higher than that at $d = 3$ μm in the potential range between $E_{tip} = -0.05$ and $E_{tip} = -0.3$ V. N_{ss} of the Sn(III) intermediate was estimated by measuring the currents on both the tip and the substrate at $E_{tip} = -0.13$ V and $E_{sub} = -0.1$ V, as shown in Figure 10a, and the N_{ss} plot as a function of L is shown in Figure 11. The tip currents were smaller even though more of the intermediate was collected as the tip was moved closer to the substrate because the amount of collected intermediate was still not enough to give a positive feedback response.[19]

Proposed Mechanism. On the basis of the CV and SECM results, we propose that the mechanism of Sn(IV) reduction can be represented as an ECEC-DISP scheme,[36] where both EC reactions involve a ligand-coupled electron transfer (LCET), involving loss of a Br^- for each electron added. The scheme is shown in Figure 12. We recognize that ambiguities can arise for complex mechanisms with many equilibrium and rate constants. Some confidence is gained by the good fits of CV data over a wide range of scan rates (Figure S3, Supporting Information). A subsequent paper devoted to the mechanism of Sn(II)−Br^- oxidation amplifies the results given here.

The final and starting Sn(IV)− and Sn(II)−bromide species in 2 M HBr + 4 M NaBr were assigned on the basis of previous studies. For Sn(II), with the known formation constants (K_1, β_{2-6}) with bromide,[37] a diagram of the fraction of Sn(II)−Br^- species (Supporting Information, Figure S5) indicates that $Sn^{II}Br_4^{2-}$ is the predominant equilibrium species under these high bromide conditions. Although there are no reports that permit the construction of a similar diagram for Sn(IV) with Br^- concentration, $Sn^{IV}Br_y^{4-y}$ was studied by Raman spectroscopy by Woodward et al.[38] In this study, the octahedral $SnBr_6^{2-}$ was the predominant species when the [total Br^-]/[total Sn^{4+}] ratio was >8 (compared to the ratio in these studies, 1200).

Simulations were performed on the basis of the following mechanism:

$$Sn^{IV}Br_6^{2-} + e^- \rightleftharpoons Sn^{III}Br_6^{3-}\ (E) \quad (11)$$

$$Sn^{III}Br_6^{3-} \rightarrow Sn^{III}Br_5^{2-} + Br^-\ (C) \quad (12)$$

$$2Sn^{III}Br_5^{2-} \rightarrow Sn^{IV}Br_5^{-} + Sn^{II}Br_5^{3-}\ (DISP) \quad (13)$$

$$Sn^{III}Br_5^{2-} + e^- \rightleftharpoons Sn^{II}Br_5^{3-}\ (E) \quad (14)$$

$$Sn^{II}Br_5^{3-} \rightarrow Sn^{II}Br_4^{2-} + Br^-\ (C) \quad (15)$$

$$Sn^{IV}Br_5^{-} + Br^- \rightarrow Sn^{IV}Br_6^{2-} \quad (16)$$

In the simulations, we assumed that the loss of Br^- in reaction 12 was fast compared to any disproportionation of $Sn^{III}Br_6^{3-}$. Moreover, the Br^- transfers in reactions 15 and 16 were assumed to be fast so that the only species that could be collected on the substrate was the Sn(III) species. Details of the simulation model are discussed in the next section. The simulation results are compared to the experimental data in Figure 11, and the best fit simulation results are given in Table 2.

The disproportionation of $2Sn^{III}Br_6^{3-}$ could be a competitive reaction with the Br^- transfer of $Sn^{III}Br_6^{3-}$ to $Sn^{III}Br_5^{2-}$, and in that case, the mechanism would be more complicated than the proposed mechanism. The main purpose of the proposed mechanism and the corresponding simulation was to show that

dx.doi.org/10.1021/ja409958a | J. Am. Chem. Soc. 2014, 136, 311−320

the intermediate detected by SECM was a Sn(III) species and that overall $Sn^{IV}Br_6^{2-}$ was electroreduced to $Sn^{II}Br_4^{2-}$ via a Sn(III) intermediate. The proposed mechanism was, therefore, simplified by taking all Br^- transfer reactions to be fast.

Savéant et al.[39] reported a concerted reductive halide cleavage mechanism for aliphatic halide compounds. In our case, however, the proposed stepwise mechanism was strongly supported by the detection of the Sn(III) intermediate by SECM in the overall electroreduction of Sn(IV).[40]

Simulation Model. Simulations were carried out with COMSOL Multiphysics v4.2a software (COMSOL, Inc., Burlington, MA), and diffusion problems were solved by the finite element method[41] under a steady-state condition. The simulation space was depicted in 2D axial symmetrical mode: a tip with a radius of 5 μm, RG = 2, and a substrate with a radius of 25 μm, RG = 2, were vertically aligned in a cylinder with a radius of 100 μm and a height of 100 μm. A depiction of the simulation model and corresponding boundary conditions in the TG/SC mode are shown in Figure 13, and the reaction mechanisms and corresponding relevant time-dependent diffusion equations in cylindrical coordinates are listed in Table 2.

CONCLUSIONS

The mechanism of Sn(IV)/Sn(II) reduction is proposed to occur via the ECEC-DISP route on the basis of the detection of a Sn(III) species as an intermediate: (1) a first et of $Sn^{IV}Br_6^{2-}/Sn^{III}Br_6^{3-}$, (2) bromide dissociation of $Sn^{III}Br_6^{3-}$ to $Sn^{III}Br_5^{2-}$, (3) a second et of $Sn^{III}Br_5^{2-}/Sn^{II}Br_5^{3-}$ in parallel with (4) disproportionation of $2Sn^{III}Br_5^{2-}$ to $Sn^{II}Br_4^{2-}$ and $Sn^{IV}Br_6^{2-}$, and (5) a second bromide dissociation of $Sn^{II}Br_5^{3-}$ to $Sn^{II}Br_4^{2-}$.

In CV, the surface peaks are attributed to Sn(0) UPD, and its desorption is attributed to $Sn(II)_{ads}$ and soluble Sn(IV) observed at $v \geq 1$ V/s. These reactions perturbed the analysis of the diffusion-controlled Sn(IV) reduction. The Sn(III)−bromide species was detected through SECM when d was a few hundred nanometers, and N_{ss} as a function of d was fitted by a COMSOL simulation based on the proposed mechanism.

ASSOCIATED CONTENT

Supporting Information

Background subtraction in fast-scan cyclic voltammograms, simulated cyclic voltammogram at 1 V/s on UME (a = 5 μm) in a diffusion-controlled one-et redox reaction, experimental and simulated cyclic voltammograms at fast scans in 60 mM Sn(IV) solution, control experiment of the Sn(III) intermediate collection by SECM with d = 3 μm in the absence of Sn(IV) species, and fraction of the composition diagram of Sn(II)−bromo species as a function of the free Br^- concentration. This material is available free of charge via the Internet at http://pubs.acs.org.

AUTHOR INFORMATION

Corresponding Author

ajbard@mail.utexas.edu

Notes

The authors declare no competing financial interest.

ACKNOWLEDGMENTS

The support of this research by the Global Climate and Energy Project (GCEP Project Number 27777240-51978A) is greatly appreciated. J.C. thanks Netzahualcóyotl Arroyo-Currás for help with the SECM experiment, Dr. Scott N. Thorgaard for discussion of the adsorption/desorption of Sn on Au, and Dr. Kevin C. Leonard for helpful discussions.

REFERENCES

(1) Khoshtariya, D. E.; Dolidze, T. D.; Zusman, L. D.; Lindbergh, G.; Glaser, J. *Inorg. Chem.* **2002**, *41*, 1728−1738.
(2) Liu, H.; Kuznetsov, A. M.; Masliy, A. N.; Ferguson, J. F.; Korshin, G. V. *Environ. Sci. Technol.* **2012**, *46*, 1430−1438.
(3) Gileadi, E. *J. Electroanal. Chem.* **2002**, *532*, 181−189.
(4) Evans, D. H. *Chem. Rev.* **2008**, *108*, 2113−2144.
(5) Bard, A. J.; Faulkner, L. R.; Kinetics of Electrode Reactions. *Electrochemical Methods, Fundamentals and Applications*, 2nd ed.; John Wiley & Sons: Hoboken, NJ, 2001; pp 107−108.
(6) Downard, A. J.; Bond, A. M.; Clayton, A. J.; Hanton, L. R.; McMorran, D. A. *Inorg. Chem.* **1996**, *35*, 7684−7690.
(7) Mandler, D.; Bard, A. J. *J. Electroanal. Chem. Interfacial Electrochem.* **1991**, *307*, 217−228.
(8) Vicente, V. A.; Bruckenstein, S. *Anal. Chem.* **1972**, *44*, 297−300.
(9) Bishop, E.; Hitchcock, P. H. *Analyst* **1973**, *98*, 635−646.
(10) Vetter, K. J. Experimental Results of Electrochemical Kinetics. *Electrochemical Kinetics. Theoretical and Experimental Aspects*; Academic Press: New York, 1967; pp 481−482.
(11) Lerner, H.; Austin, L. G. *J. Electrochem. Soc.* **1965**, *112*, 636.
(12) (a) Shinohara, N.; Mori, K.; Inoue, M. *Chem. Lett.* **1986**, *15*, 661−664. (b) Shinohara, N.; Inoue, M. *Bull. Chem. Soc. Jpn.* **1989**, *62*, 730−733.
(13) Jiang-Tsu, Y.; Ssu-Hao, L.; Yng-Huey, J.; Ching-Jiun, W. *J. Phys. Chem. Solids* **1993**, *54*, 57−64.
(14) (a) Pierce, D. T.; Geiger, W. E. *J. Am. Chem. Soc.* **1992**, *114*, 6063−6073. (b) Stoll, M. E.; Belanzoni, P.; Calhorda, M. J.; Drew, M. G. B.; Félix, V.; Geiger, W. E.; Gamelas, C. A.; Gonçalves, I. S.; Romão, C. C.; Veiros, L. F. *J. Am. Chem. Soc.* **2001**, *123*, 10595−10606. (c) Kaim, W.; Reinhardt, R.; Greulich, S.; Fiedler, J. *Organometallics* **2003**, *22*, 2240−2244.
(15) Mirkin, M. V.; Yang, H. J.; Bard, A. J. *J. Electrochem. Soc.* **1992**, *139*, 2212−2217.
(16) (a) Yang, H.; Bard, A. J. *J. Electroanal. Chem. Interfacial Electrochem.* **1991**, *306*, 87−109. (b) Yang, H.; Bard, A. J. *J. Electroanal. Chem.* **1992**, *339*, 423−449. (c) Yang, H.; Wipf, D. O.; Bard, A. J. *J. Electroanal. Chem.* **1992**, *331*, 913−924. (d) Baur, J. E.; Wang, S.; Brandt, M. C. *Anal. Chem.* **1996**, *68*, 3815−21. (e) Andrieux, C. P.; Hapiot, P.; Saveant, J. M. *J. Phys. Chem.* **1988**, *92*, 5987−5992. (f) Andrieux, C. P.; Audebert, P.; Hapiot, P.; Saveant, J. M. *J. Am. Chem. Soc.* **1990**, *112*, 2439−2440.
(17) Bard, A. J.; Fan, F.-R. F.; Kwak, J.; Lev, O. *Anal. Chem.* **1989**, *61*, 132−138.
(18) Zhou, F.; Bard, A. J. *J. Am. Chem. Soc.* **1994**, *116*, 393−394.
(19) Bi, S.; Liu, B.; Fan, F.-R. F.; Bard, A. J. *J. Am. Chem. Soc.* **2005**, *127*, 3690−3691.
(20) Bard, A. J. Introduction and Principles. In *Scanning Electrochemical Microscopy*; Mirkin, M. V., Bard, A. J., Eds.; Marcel Dekker: New York, 2001; pp 1−9.
(21) (a) Skyllas-Kazacos, M.; Chakrabarti, M. H.; Hajimolana, S. A.; Mjalli, F. S.; Saleem, M. *J. Electrochem. Soc.* **2011**, *158*, R55−R79. (b) Skyllas-Kazacos, M. *J. Power Sources* **2003**, *124*, 299−302.
(22) Fan, F.-R. F.; Demaille, C. The Preparation of Tips for Scanning Electrochemical Microscopy. In *Scanning Electrochemical Microscopy*; Mirkin, M. V., Bard, A. J., Eds.; Marcel Dekker: New York, 2001; pp 75−78.
(23) Chang, J.; Leonard, K. C.; Cho, S. K.; Bard, A. J. *Anal. Chem.* **2012**, *84*, 5159−5163.
(24) Denuault, G.; Mirkin, M. V.; Bard, A. J. *J. Electroanal. Chem. Interfacial Electrochem.* **1991**, *308*, 27−38.
(25) Heinze, J. *Angew. Chem., Int. Ed. Engl.* **1993**, *32*, 1268−1288.
(26) Wopschall, R. H.; Shain, I. *Anal. Chem.* **1967**, *39*, 1514−1527.
(27) Fonticelli, M.; Tucceri, R. I.; Posadas, D. *Electrochim. Acta* **2004**, *49*, 5197−5202.

(28) Qiao, Z. Q.; Shang, W.; Zhang, X.; Wang, C. M. *Anal. Bioanal. Chem.* **2005**, *381*, 1467−1471.
(29) Rodes, A.; Feliu, J. M.; Aldaz, A.; Clavilier, J. *J. Electroanal. Chem. Interfacial Electrochem.* **1988**, *256*, 455−462.
(30) Mao, B.-W.; Tang, J.; Randler, R. *Langmuir* **2002**, *18*, 5329−5332.
(31) Bakos, I.; Szabó, S. *Electrochim. Acta* **2001**, *46*, 2507−2513.
(32) Mallory, G. O. The Fundamental Aspects of Electroless Nickel Plating. In *Electroless Plating: Fundamentals and Applications*; Mallory, G. O., Hajdu, J. B., Eds.; American Electroplates and Surface Finishers Society: Orlando, FL, 1996; pp 19−20.
(33) Bard, A. J.; Faulkner, L. R. Scanning Probe Techniques. *Electrochemical Methods, Fundamentals and Applications*, 2nd ed.; John Wiley & Sons: Hoboken, NJ, 2001; pp 670−673.
(34) Unwin, P. R. Kinetics of Homogeneous Reactions Coupled to Heterogeneous Electron Transfer. In *Scanning Electrochemical Microscopy*; Mirkin, M. V., Bard, A. J., Eds.; Marcel Dekker: New York, 2001; pp 244−254.
(35) Shen, M.; Arroyo-Currás, N.; Bard, A. J. *Anal. Chem.* **2011**, *83*, 9082−9085.
(36) (a) Costentin, C.; Robert, M.; Savéant, J.-M. *Chem. Rev.* **2010**, *110*, PR1−PR40. (b) Demaille, C.; Unwin, P. R.; Bard, A. J. *J. Phys. Chem.* **1996**, *100*, 14137−14143.
(37) Högfeldt. E. *Stability Constants of Metal-Ion Complexes, Part A: Inorganic Ligands*, 1st ed.; IUPAC Chemical Data Series, No. 21; Pergamon Press: New York, 1982; p 264.
(38) Woodward, L. A.; Anderson, L. E. *J. Chem. Soc.* **1957**, 1284−1286.
(39) (a) Andrieux, C. P.; Le Gorande, A.; Savéant, J.-M. *J. Am. Chem. Soc.* **1992**, *114*, 6892−6904. (b) Andrieux, C. P.; Differding, E.; Robert, M.; Savéant, J.-M. *J. Am. Chem. Soc.* **1993**, *115*, 6592−6599. (c) Andrieux, C. P.; Savéant, J.-M.; Tallec, A.; Tardivel, R.; Tardy, C. *J. Am. Chem. Soc.* **1997**, *119*, 2420−2429. (d) Savéant, J.-M. *J. Am. Chem. Soc.* **1992**, *114*, 10595−10602. (e) Andrieux, C. P.; Combellas, C.; Kanoufi, F.; Savéant, J.-M.; Thiébault, A. *J. Am. Chem. Soc.* **1997**, *119*, 9527−9540.
(40) Savéant, J.-M. Electron Transfer, Bond Breaking, and Bond Formation. *Elements of Molecular and Biomolecular Electrochemistry*, 1st ed.; John Wiley & Sons: Hoboken, NJ, 2006; pp 203−217.
(41) Peaceman, D. W.; Pachford, H. H. *J. Soc. Ind. Appl. Math.* **1955**, *3*, 28−41.